

1 **Sea ice  $p\text{CO}_2$  dynamics and air-ice  $\text{CO}_2$  fluxes during the SIMBA**

2 **Experiment – Bellingshausen Sea, Antarctica**

3  
4 Geilfus N.-X.<sup>1,2,3</sup>, Tison J.-L.<sup>2</sup>, Ackley S.F.<sup>4</sup>, Galley R.J.<sup>5</sup>, Rysgaard S.<sup>1,5,6</sup>, Miller L.A.<sup>7</sup> and Delille  
5 B.<sup>3</sup>

6  
7 <sup>1</sup> Arctic Research Centre, Aarhus University, Aarhus, Denmark

8 <sup>2</sup> Laboratoire de Glaciologie, Université Libre de Bruxelles, Bruxelles, Belgium

9 <sup>3</sup> Unité d'Océanographie Chimique, Université de Liège, Liège, Belgium

10 <sup>4</sup> Department of Geological Sciences, University of Texas at San Antonio, San Antonio, TX,  
11 USA

12 <sup>5</sup> Centre for Earth Observation Science, University of Manitoba, Winnipeg, Canada

13 <sup>6</sup> Greenland Climate Research Centre, Greenland Institute of Natural Resources, Nuuk,  
14 Greenland

15 <sup>7</sup> Centre for Ocean Climate Chemistry, Institute of Ocean Sciences, Fisheries and Oceans,  
16 Canada, Sidney, BC, Canada.

17 Keywords: sea ice, snow,  $\text{CO}_2$ , Antarctic,  $\text{CO}_2$  fluxes

18

## 19      **1. Abstract**

20            Temporal evolution of  $p\text{CO}_2$  profiles in sea ice in the Bellingshausen Sea,  
21            Antarctica, in October 2007 shows physical and thermodynamic processes controls  
22            the  $\text{CO}_2$  system in the ice. During the survey, cyclical warming and cooling strongly  
23            influenced the physical, chemical and thermodynamic properties of the ice cover.  
24            Two sampling sites with contrasting characteristics of ice and snow thickness were  
25            sampled: one had little snow accumulation (from 8 to 25 cm) and larger temperature  
26            and salinity variations than the second site, where the snow cover was up to 38 cm  
27            thick and therefore better insulated the underlying sea ice. We show that each  
28            cooling/warming event was associated with an increase/decrease in the brine  
29            salinity, total alkalinity (TA), total dissolved inorganic carbon ( $\text{TCO}_2$ ), and *in situ*  
30            brine and bulk ice  $\text{CO}_2$  partial pressures ( $p\text{CO}_2$ ). Thicker snow covers reduced the  
31            amplitude of these changes: snow cover influences the sea ice carbonate system by  
32            modulating the temperature and therefore the salinity of the sea ice cover. Results  
33            indicate that  $p\text{CO}_2$  was undersaturated with respect to the atmosphere both in the *in*  
34            *situ* bulk ice (from 10 to 193  $\mu\text{atm}$ ), and brine (from 65 to 293  $\mu\text{atm}$ ), causing the sea  
35            ice to act as a sink for atmospheric  $\text{CO}_2$  (up to 2.9  $\text{mmol m}^{-2} \text{d}^{-1}$ ), despite  
36            supersaturation of the underlying seawater (up to 462  $\mu\text{atm}$ ).

## 37 2. Introduction

38 Sea ice formation and melting may have a strong impact on the carbon cycle of  
39 polar oceans [e.g., *Rysgaard et al.*, 2011, *Delille et al.*, 2014]. However, processes  
40 related to freezing and melting of sea ice, as well as their impact on CO<sub>2</sub> exchanges  
41 with the atmosphere, are still poorly understood [*Parmentier et al.*, 2013]. Detailed  
42 studies have been conducted on sea ice inorganic carbon chemistry and the impact  
43 of sea ice on the carbon cycle and the CO<sub>2</sub> exchanges between atmosphere, sea ice,  
44 and the ocean over the last decade [*Semiletov et al.*, 2004; *Zemmelink et al.*, 2006;  
45 *Rysgaard et al.*, 2007; 2011; 2012; *Delille et al.*, 2007; 2014; *Miller et al.*, 2011,  
46 *Papakyriakou and Miller* 2011; *Geilfus et al.*, 2012a; 2013; *Nomura et al.*, 2010a;  
47 2013]. These studies have shown that in both hemispheres, CO<sub>2</sub>-carbonate chemistry  
48 in sea ice and brine is heterogeneous and variable, resulting in complex CO<sub>2</sub>  
49 dynamics.

50 The CO<sub>2</sub> chemistry of sea ice seems to be highly dependent on brine salinity,  
51 which is controlled by ice temperature [*Weeks*, 2010]. Both brine concentration  
52 during ice growth and brine dilution during ice melt play major roles in the  
53 carbonate system dynamics within sea ice [*Papadimitriou et al.*, 2004; *Nomura et al.*,  
54 2010a; *Geilfus et al.*, 2012a]. In parallel, temperature dependence of both the  
55 dissociation constants of the carbonate system and the Henry's Law constant for CO<sub>2</sub>  
56 affect *p*CO<sub>2</sub> in sea ice. Brine concentration/dilution can be associated with  
57 precipitation/dissolution of calcium carbonate within the sea ice, also promoting an  
58 increase/decrease in the *in situ* brine *p*CO<sub>2</sub> [*Papadimitriou et al.*, 2004; 2008;  
59 *Rysgaard et al.*, 2007; 2012; 2013; *Geilfus et al.*, 2012a; 2013]. Primary production

60 and respiration can also affect the CO<sub>2</sub>-carbonate system within sea ice [*Thomas and*  
61 *Dieckmann 2010; Dieckmann and Hellmer, 2010; Delille et al., 2007*]. Finally, brine  
62 and gas transport within sea ice and across the air-ice and ice-water interfaces  
63 affect TA, TCO<sub>2</sub>, and CO<sub>2</sub> distributions within the ice, together with the overall  
64 amount of CO<sub>2</sub> in the sea ice. The role of ice-covered oceans in the CO<sub>2</sub> balance has  
65 been largely ignored because continuous sea ice cover is assumed to impede gaseous  
66 exchange with the atmosphere. However, recent studies show that sea ice may  
67 mediate the air to sea CO<sub>2</sub> transfer. Understanding of the seasonal and geographical  
68 conditions of the inorganic carbon dynamics related with sea ice is limited. The main  
69 goal of this study is to add to the still limited database on inorganic carbon dynamic  
70 in ice-covered seas.

71 Although snow thickness and distribution are variable and primarily result from  
72 wind-induced redistribution during storms [*Weeks 2010*], the impact of snow cover  
73 on the thermal evolution of sea ice can be significant [*Massom et al., 2001*]. Snow,  
74 which has a low thermal conductivity compared to sea ice [*Massom et al., 2001*],  
75 provides thermal insulation between the cold air and the ice. The presence of a thick  
76 snow cover also affects the isostatic balance, potentially resulting in negative  
77 freeboard (i.e. the snow-ice interface is submerged below the seawater level). If the  
78 sea ice is permeable throughout the entire ice column, negative freeboard causes  
79 vertical flooding to at least the snow-ice interface through open brine channels. The  
80 percolation threshold above which columnar sea ice is considered permeable to fluid  
81 transport corresponds to a brine volume (which is controlled by temperature and  
82 salinity) of 5% [*Golden et al., 1998; 2007*].

83           Therefore, snow accumulation could impact the CO<sub>2</sub>-carbonate system within  
84 sea ice by regulating the ice temperature and the extent of flooding. The impact of  
85 snow on the CO<sub>2</sub> exchanges between sea ice and the atmosphere has previously been  
86 discussed by *Nomura et al.*, [2010b]; these authors suggested that a snow cover  
87 thicker than 9 cm could prevent any sea ice-atmosphere exchanges of CO<sub>2</sub> and that  
88 melting snow can act as a physical barrier to CO<sub>2</sub> fluxes.

89           In this study, we examine the temporal evolution of *in situ* brine and bulk ice *p*CO<sub>2</sub>  
90 profiles associated with physical and biogeochemical variables in the sea ice cover of  
91 two contrasting study sites, named “Brussels” and “Liège” between 1 and 23 October  
92 2007, during the Sea Ice Mass Balance in Antarctic (SIMBA) cruise (Bellingshausen  
93 Sea, Antarctica) (Figure 1) [*Lewis et al.*, 2011]. Further, we differentiate the  
94 dynamics of *in situ* brine and bulk ice *p*CO<sub>2</sub>. Sea ice temperature and bulk salinity  
95 differences at these two stations, in part due to substantial difference in snow cover,  
96 impact the inorganic carbon dynamics within sea ice and its brine and the related  
97 air-ice CO<sub>2</sub> fluxes.

### 98   **3. Study site, materials and methods**

#### 99       **a. Selection of study site**

100           The Sea Ice Mass Balance in the Antarctic (SIMBA) cruise investigated the  
101 physical and biological interactions between the ocean, sea ice, snow cover and  
102 atmosphere in the Bellingshausen Sea, onboard the RV *Nathaniel B. Palmer* (NBP) in  
103 October 2007. During this ~ one-month experiment, the vessel was moored to a first  
104 year sea-ice floe, the Ice Station Belgica (ISB), south of Peter I Island, at  
105 approximately 69-71°S and 90-95°W (Figure 1). The station was chosen for its wide

106 variety of ice types and snow cover [Lewis *et al.*, 2011], characteristic of the greater  
107 region and the size of the ice floe ( $\sim 5 \text{ km}^2$ ) was deemed large enough to survive the  
108 duration of the field experiment. Sampling was conducted at two distinct sites based  
109 on: (i) homogeneity of the surface properties within each site, to reduce within-site  
110 spatial variability; (ii) the contrast in ice and snow properties between the two  
111 chosen sites; and (iii) maximum distance from the ship (0.8 km and 1.1 km), to  
112 prevent sample contamination. Each site was 100x60 m and subdivided into small  
113 work sub-areas approximately 5m x 5m. The 25 m<sup>2</sup> sub-areas were located adjacent  
114 to each other to minimize spatial variability [Lewis *et al.*, 2011]. Each station was  
115 sampled at 5-day intervals: the Brussels site (low snow cover, at 0.8 km) was  
116 sampled on 1, 6, 11, 16, and 21 October and the Liège site (high snow cover, at 1.1  
117 km) was sampled on 3, 8, 13, 18, and 23 October (Figure 2).

## 118 **b. Sampling procedures**

119 Ice cores were collected using an electro-polished stainless steel corer (14 cm  
120 diameter) using an electric drill head, connected by a long cord to a power supply  
121 generator located downwind. Cores were immediately wrapped in polyethylene bags  
122 and placed in an insulated box filled with gel packs pre-cooled to  $-30^\circ\text{C}$  in order to  
123 limit brine drainage from samples [Tison *et al.*, 2008] and brought back to the ship  
124 laboratory. Sackholes [Gleitz *et al.*, 1995] for collecting brine were drilled to four  
125 depths: 15, 30, 40, and 50 cm at the Brussels site; and 15, 30, 60 and 90 cm at the  
126 Liège site. Each sackhole was covered with a plastic lid to prevent contamination by  
127 falling snow. Brine seeped into the sackholes for 10 to 60 min before collection using  
128 a peristaltic pump (Cole Palmer, Masterflex-Environmental Sampler). Under-ice

129 seawater was collected using the same peristaltic pump, with the inlet positioned at  
130 the ice–water interface, and at 1 and 30 m depths. On each sampling date, ice cores,  
131 brine and seawater were collected and analyzed for a full range of physical and  
132 biogeochemical variables: temperature (T), salinity (S), water stable isotopes of  $\delta^{18}\text{O}$ ,  
133 chlorophyll *a* (Chl *a*), total alkalinity (TA),  $\text{pH}_T$ , and *in situ*  $\text{CO}_2$  partial pressure  
134 ( $p\text{CO}_2$ ). Brine samples for  $\text{pH}_T$  and TA analyses were only collected from the  
135 shallowest sackhole depth (at 0 to 15 cm) and at 0 to 40 cm depth at the Brussels site  
136 and 0 to 60 cm depth at the Liège site sackholes.

### 137 **c. Materials and methods**

138 The ice temperature was measured immediately after extraction of the ice core  
139 using a calibrated temperature probe (TESTO 720,  $\pm 0.1^\circ\text{C}$  precision) inserted into  
140 pre-drilled holes ( $\sim 5$  cm intervals) perpendicular to the core sides. In the field, the  
141 ice core dedicated to bulk ice salinity measurements was cut into 5 cm thick slices  
142 which were stored in separate, closed containers. These ice samples were melted at  
143 room temperature on board and bulk ice salinity on the practical salinity scale was  
144 determined from conductivity and temperature using a portable calibrated Orion 3-  
145 Star conductivity meter (precision of  $\pm 0.1$ ). Samples with salinity higher than 42  
146 were diluted with ultrapure water using an analytical balance. Brine volumes  
147 profiles were calculated for each core using these bulk ice salinities and ice  
148 temperatures according to *Cox and Weeks* [1983] for ice temperatures below  $-2^\circ\text{C}$   
149 and according to *Leppäranta and Manninen* [1988] for ice temperatures within the  
150 range  $-2^\circ\text{C}$  to  $0^\circ\text{C}$ . Calculated brine salinity profiles were determined from the *in situ*  
151 ice temperatures (after *Cox and Weeks* [1983]).

152 Aliquots (10 ml) of the bulk melted sea ice samples were transferred to gas tight  
153 vials for  $\delta^{18}\text{O}$  measurements at the Australian Antarctic CRC. Isotope ratios were  
154 measured with a dual-inlet VG SIRA mass spectrometer using the conventional  
155 water- $\text{CO}_2$  equilibration method (accuracy with respect to VSMOW =  $\pm 0.12 \text{ ‰}$ ).

156 The pH of the sea-ice brine and seawater was measured using a Metrohm  
157 combined electrode calibrated on the total hydrogen ion scale ( $\text{pH}_T$ ) using TRIS (2-  
158 amino-2-hydroxymethyl-1.3-propanediol) and AMP (2-aminopyridine) buffers  
159 prepared at salinities of 35 and 75 according to the formulations proposed by *DOE*  
160 [1994]. Samples were maintained as close as possible to their in situ temperature  
161 (typically below  $3^\circ\text{C}$ ), and measurements of  $\text{pH}_T$  were carried out as soon as possible  
162 after upon return to the ship laboratory (typically less than 2 hours after sampling).  
163 The pH electrode was calibrated at temperatures ranging from 0 to  $4^\circ\text{C}$  and at  
164 salinities ranging from 35 to 75. The accuracy of the  $\text{pH}_T$  measurements was  $\pm 0.01$   
165 pH unit [*Frankignoulle and Borges, 2001*].

166 Total alkalinity in the brine and underlying seawater was measured by open-cell  
167 titration with HCl 0.1M, and the endpoints were determined according to *Gran*  
168 [1952]. Routine analyses of Certified Reference Materials provided by A. G. Dickson,  
169 Scripps Institution of Oceanography, verified that the error in these TA data was  
170 smaller than  $\pm 4 \text{ } \mu\text{mol kg}^{-1}$ . Total inorganic carbon ( $\text{TCO}_2$ ) and  $\text{pCO}_2$  (denoted as  
171  $\text{pCO}_{2\text{calc}}$ ) were calculated from TA and  $\text{pH}_T$  using the  $\text{CO}_2$  acidity constants of  
172 *Mehrbach et al.*, [1973] refit by *Dickson and Millero* [1987] and other constants  
173 advocated by *DOE* [1994]. We assumed that the  $\text{CO}_2$  dissociation constants were



174 applicable at subzero temperatures as suggested by *Marion* [2001] and *Delille et al.*,  
175 [2007].

176 Brine and underlying seawater  $p\text{CO}_2$  were measured *in situ* using a custom-made  
177 equilibration system [*Geilfus et al.*, 2012a]. The system consisted of a membrane  
178 contactor equilibrator (Membrana, Liqui-cell) connected to a non-dispersive infrared  
179 gas analyzer (IRGA, Li-Cor 6262) via a closed air loop. Brine and airflow rates from  
180 the equilibrator and IRGA were approximately  $2 \text{ L min}^{-1}$  and  $3 \text{ L min}^{-1}$  respectively.  
181 Temperature was measured within the sackholes or under-ice water and at the  
182 equilibrator outlet simultaneously using Li-Cor temperature sensors. The  $p\text{CO}_2$   
183 values were temperature-corrected assuming that the *Copin Montégut* [1988]  
184 relation is valid at low temperatures and high salinities. The IRGA was calibrated  
185 immediately upon returning to the ship while the analyzer was still cold. All devices,  
186 except the peristaltic pump, were enclosed in an insulated box that contained a 12 V  
187 power source providing enough heat to keep the inside temperature just above  $0^\circ\text{C}$ .

188 Ice cores were kept frozen during storage and shipping for subsequent analysis  
189 of bulk ice  $p\text{CO}_2$  at the Laboratoire de Glaciologie, Université Libre de Bruxelles,  
190 Belgium. The general principle of the method was to equilibrate the sea ice samples  
191 at the *in situ* temperature with a mixture of  $\text{N}_2$  and  $\text{CO}_2$  at known concentrations (so-  
192 called standard gas,  $396 \mu\text{atm}$ ) and rapidly extract the gas into a Varian 3300 gas  
193 chromatograph under vacuum [*Geilfus et al.*, 2012b]. Each ice sample was cut into a 4  
194 x 4 x 4.5 cm cube to tightly fit the equilibration container, thereby both minimizing  
195 the headspace and keeping it consistent. The standard gas was injected at 1013 mbar  
196 into the equilibration container containing the ice sample. Then the container with

197 the ice sample is placed in a thermostatic bath setup at the field *in situ* temperature  
198 for 24 hours. This timing is chosen to ensure that the sample is re-equilibrated to the  
199 brine volume and chemical conditions at the *in situ* temperature. A quick injection  
200 into the gas chromatograph then allows the reconstruction of the equilibrium brine  
201  $p\text{CO}_2$  at the *in situ* temperature. This method is only valid if the ice is permeable at  
202 the *in situ* conditions [Geilfus et al., 2012b] and microstructure changes resulting  
203 from cooling during storage and warming prior to analysis are assumed to have a  
204 minor impact on the bulk ice  $p\text{CO}_2$ .

205 Air-ice  $\text{CO}_2$  fluxes were measured using an accumulation chamber (West  
206 System) placed on top of the ice. The chamber was a metal cylinder closed at the top,  
207 with an internal diameter of 20 cm and an internal height of 9.7 cm. A rubber seal  
208 surrounded by a serrated steel edge ensured an airtight connection between the ice  
209 and the chamber. Over snow, a steel tube was mounted at the base of the chamber to  
210 enclose the snowpack to the ice surface and prevent lateral infiltration of air into the  
211 chambered volume of snow. The chamber was connected in a closed loop to the IRGA  
212 with an air pump rate of  $3 \text{ L min}^{-1}$ . The  $p\text{CO}_2$  in the chamber was recorded every 30  
213 sec for a minimum of 5 min. The flux was computed from the slope of the linear  
214 regression of  $p\text{CO}_2$  versus time ( $r^2 > 0.99$ ) according to Frankignoulle [1988], taking  
215 into account the volume of ice or snow enclosed within the chamber. The average  
216 uncertainty of the flux computation due to the standard error of the regression slope  
217 was  $\pm 3\%$ .

## 218 **4. Results**

219           **a. Atmospheric conditions**

220           During the 2007 winter–spring transition in the Bellingshausen Sea, several low-  
221           pressure systems of varying intensity and length occurred at the sampling location.  
222           Fluctuations in the air temperature are shown in Figure 3, along with the surface ice  
223           temperature measured at each station. At least three successive cycles of warming  
224           and cooling were recorded with air temperatures ranging from 0.5°C to -20°C. These  
225           cycles consisted of warm atmospheric fronts from the north, generally accompanied  
226           by high velocity winds and precipitation, followed by cold air temperatures and little  
227           precipitation [*Lewis et al., 2011; Vancoppenolle et al., 2011*].

228           **b. Sea ice and snow conditions**

229           The Brussels and Liège sites had contrasting conditions in snow, ice thickness  
230           (Figure 2) and ice texture, which are presented in detail by *Lewis et al., [2011]*.

231           At the Brussels site, the ice thickness, as determined by coring, ranged from 55  
232           to 67 cm, while the snow cover ranged from 8 to 25 cm (Figure 2a). The ice  
233           freeboard was positive and ranged from 0.7 to 3 cm. The ice cover was mainly  
234           composed of columnar crystals [*Lewis et al., 2011*]. The ice temperatures ranged  
235           from -1.5 to -6.1°C (Figure 4). The main changes in temperatures were observed in  
236           the top 40 cm of the ice cover, oscillating between cooling and warming events  
237           within a 1°C temperature window (from -3°C to -4°C), except on 16 October, when  
238           the near-surface ice temperature decreased to -6.1°C and the top 40 cm reached it's  
239           minimum observed temperature. The bulk ice salinity ranged from 3.4 to 14.1. The  
240           profiles were typically S-shaped, as described by *Eicken [1992]*, with higher salinities

241 (from 11.5 to 14.1) in the top layer, dropping to minimum values (on average,  $S =$   
242 4.1) at the bottom. Between 1 and 16 October, the brine salinities increased from the  
243 bottom to the top of the ice cover, with values close to seawater ( $S=34$ ) at the bottom  
244 to a maximum of 101 at the top on 16 October. The brine volume was always greater  
245 than 5%, except in the top 20 cm of the ice cover on 16 October. The  $\delta^{18}\text{O}$  isotopic  
246 ratio ranged from -5.8 ‰ to 2.1 ‰. The top 15 cm showed negative  $\delta^{18}\text{O}$  values at  
247 each sample interval, while the rest of the profile was increasing steadily towards a  
248 value of +2 ‰ at the bottom.

249 At the Liège site, the ice and snow cover were thicker than at the Brussels site  
250 and ranged from 99 to 106 cm and from 28 to 38 cm, respectively (Figure 2b). The  
251 ice freeboard was negative on 18 and 23 October, flooding the snow–ice interface.  
252 The ice cover at the Liège site was mainly composed of granular sea ice with  
253 inclusions of columnar and snow ice layers at different levels in the ice profile (see  
254 *Lewis et al.*, [2011] for a detailed description of the ice texture profile at the Liège  
255 site). These inclusions, associated with sharp excursions in the  $\delta^{18}\text{O}$  ratios (Figure 4),  
256 indicate a history of dynamic conditions and repeated subsequent rafting events  
257 [*Lewis et al.*, 2011]. The observed variations of the bulk ice temperature and salinity,  
258 as well as the calculated brine salinity, were smaller than those observed at Brussels  
259 (Figure 4). The ice temperature ranged from -1.3°C to -3.7°C. The ice cover showed  
260 similar warm and isothermal profiles on 3, 8 and 23 October, with brine salinities  
261 close to seawater values throughout the ice column. The ice cover cooled from 8 to  
262 18 October, when the minimum temperature and maximum brine salinity were  
263 observed, as we also observed at the Brussels site. The bulk ice salinity ranged from

264 2.3 to 13.8, and the salinity profiles were also typically S-shaped, with the top layer  
265 ranging from 6.5 to 13.8, while the average salinity of the bottom layer was 3. The  
266 calculated brine volume fraction was always above 5%. The  $\delta^{18}\text{O}$  ratios ranged from  
267  $-4.9\text{‰}$  to  $2.9\text{‰}$ . At the top of the ice,  $\delta^{18}\text{O}$  was negative from 3 to 13 October and  
268 positive on our last two sampling days. In the lower half of the profiles,  $\delta^{18}\text{O}$  values  
269 were generally around  $1\text{‰}$ , although the cores sampled on 18 and 23 October had  
270 negative  $\delta^{18}\text{O}$  intervals, further indicative of ice rafting.

### 271 **c. Carbonate system**

272 At the Brussels site, TA in brine sampled from sackholes ranged from 2406 to  
273  $4855\ \mu\text{mol kg}^{-1}$  while  $TCO_2$  ranged from 2288 to  $4110\ \mu\text{mol kg}^{-1}$  (Figure 5). Changes  
274 in TA and  $TCO_2$  closely mimicked the salinity changes. Normalizing TA and  $TCO_2$  to a  
275 salinity of 34 (denoted as  $nTA$  and  $nTCO_2$ ) indicate the sensitivity of these  
276 parameters to salinity changes; both  $nTA$  and  $nTCO_2$  remain relatively stable ( $2350$   
277  $\mu\text{mol kg}^{-1}$  and  $2010\ \mu\text{mol kg}^{-1}$  respectively). The  $pH_T$  ranged from 7.9 to 8.8 and  
278 increased continuously during the survey, except for a significant decrease in the  
279 deeper brine on 16 October (Figure 5) associated with decreased brine salinity and  
280 TA. The *in situ* brine  $pCO_2$  ranged from 82 to  $392\ \mu\text{atm}$ . Brine was undersaturated in  
281  $CO_2$  relative to the atmosphere ( $383.8\ \mu\text{atm}$  in 2007), except on 16 October (Figure  
282 5, 6). The brine  $pCO_{2\text{calc}}$  was similar to brine  $pCO_2$  measured *in situ* ( $\pm 50\ \mu\text{atm}$ ),  
283 except on 1 October when brine  $pCO_{2\text{calc}}$  was extremely high ( $620\ \mu\text{atm}$ , Figure 5).  
284 From 1 to 6 October, the *in situ* brine  $pCO_2$  values were from 210 to  $271\ \mu\text{atm}$  (Figure  
285 6). Then, the *in situ* brine  $pCO_2$  decreased on 11 October and increased again on 16  
286 October to concentrations ranging from 248 to  $392\ \mu\text{atm}$ . On 21 October, the *in situ*

287 brine  $p\text{CO}_2$  decreased down to concentrations ranging from 82 to 115  $\mu\text{atm}$ . The bulk  
288 ice  $p\text{CO}_2$  ranged from 15 to 150  $\mu\text{atm}$  (Figure 6), generally increasing with depth and  
289 lower or equal to the brine  $p\text{CO}_2$ .

290 At the Liège site, the brine salinity ranged from 38.1 to 58.3. TA ranged from  
291 2806 to 4074  $\mu\text{mol kg}^{-1}$  while  $\text{TCO}_2$  ranged from 1826 to 3590  $\mu\text{mol kg}^{-1}$  (Figure 5).  
292 As for the Brussels site, TA and  $\text{TCO}_2$  changes seem closely related to salinity  
293 changes, except on 3 October. The  $\text{pH}_T$  ranged from 8.5 to 8.7 with a significant  
294 increase on 13 October to a maximum of 9.2 (Figure 5). The *in situ* brine  $p\text{CO}_2$  was  
295 undersaturated compared to the atmosphere, with values ranging from 65 to 183  
296  $\mu\text{atm}$ . These values were consistent with the brine  $p\text{CO}_{2\text{calc}}$  ( $\pm 80 \mu\text{atm}$ ) Changes of  
297 the *in situ* brine  $p\text{CO}_2$  were smaller than the variations at the Brussels site. The most  
298 significant change occurred on 18 October where the *in situ* brine  $p\text{CO}_2$  increased to  
299 concentrations ranging from 147 to 183  $\mu\text{atm}$ . The bulk ice  $p\text{CO}_2$  ranged from 9 to  
300 193  $\mu\text{atm}$  (Figure 6). Bulk ice  $p\text{CO}_2$  were here generally more consistent with brine  
301  $p\text{CO}_2$ , except in the colder 8 and 18 October stations. The minimum concentrations  
302 were observed in the top 20 cm of the ice cover while the maximum concentrations  
303 were observed at the sea ice interface with the underlying seawater. The mean bulk  
304 ice  $p\text{CO}_2$  ranged from 70 to 79  $\mu\text{atm}$  from 3 to 18 October and increased to 97  $\mu\text{atm}$   
305 on 23 October.

306 The salinity and  $\text{CO}_2$  system parameters were relatively constant in the  
307 underlying seawater during our survey (Figure 7). We observed a slight decrease in  
308 the salinity on 13 October, while  $\text{pH}_T$  decreased and  $\text{TCO}_2$  increased on 11 and 13

309 October. The seawater  $p\text{CO}_2$  measured *in situ* was supersaturated relative to the  
310 atmosphere, ranging from 401 to 462  $\mu\text{atm}$ .

#### 311 **d. Air-ice $\text{CO}_2$ fluxes**

312 The  $\text{CO}_2$  fluxes measured at the sea ice and snow interfaces with the atmosphere  
313 suggest that, except for a small efflux of  $0.3 \text{ mmol m}^{-2} \text{ d}^{-1}$  measured over the ice at  
314 the Brussels site on 16 October, both the sea ice and the snow acted as sinks for  
315 atmospheric  $\text{CO}_2$  during our study (Figure 8). In general, Brussels sea ice showed a  
316 small uptake of atmospheric  $\text{CO}_2$  that was not significantly different from zero  
317 (Figure 8a). At Liège, the uptake of atmospheric  $\text{CO}_2$  was more substantial, ranging  
318 up to  $-2.9 \text{ mmol m}^{-2} \text{ d}^{-1}$  over sea ice with smaller values over snow covered ice  
319 (Figure 8b).

## 320 **5. Discussion**

### 321 a. Impact of atmospheric forcing and snow thickness on the physical properties 322 of the ice cover

323 At the beginning of the sampling period the ice cover at stations Brussels and Liège  
324 were nearly isothermal. Subsequently, successive warm and cold events associated  
325 with passing atmospheric fronts (Figure 3) affected the temperature gradient within  
326 the ice cover significantly. At both sites, the fluctuations in ice temperature occurred  
327 mainly in the top 40 cm (Figure 4). The high brine salinities associated with the cold  
328 ice temperature at the top of the ice resulted in an unstable salinity gradient within  
329 the ice cover (Figure 4). This may have initiated overturning of brine and the mixing  
330 with underlying seawater with brine moving downward through the ice cover to be

331 replaced by underlying seawater moving upward [Lewis et al., 2011]. To confirm this  
332 hypothesis, Lewis et al., [2011] reported presence of dissolution features observed  
333 on freshly extracted ice cores and thick sections as well as under-ice photographs  
334 clearly showing brine drainage at the ice bottom. Brine convection is driven by the  
335 density difference between high-salinity brine in the ice and the seawater  
336 underneath. Its onset and strength can be described by the mushy-layer Rayleigh  
337 numbers (Ra)[Wettlaufer et al., 1997]. Ra numbers provided by Brabant [2012]  
338 suggests that brine drainage occurred at the Brussels site between 1 and 6 October  
339 (Ra >10) and between 11 and 16 October (6<Ra<7) which is also confirmed by  
340 vertical nutrient distribution in the sea ice [Brabant 2012]. At the Liège site, thicker  
341 snow muted thermal fluctuations within the sea ice reducing the magnitude of  
342 changes in brine volume and salinity. Hence, the variations in brine salinity and in  
343 the resulting density gradient were more moderate at Liège (Figure 4), resulting in a  
344 lower Ra [Brabant 2012]. It is also possible that some natural intra-site variability  
345 within the sea ice existed at the two sampling locations. Given the textural evidence  
346 of dynamic processes at Liège [Lewis et al., 2011] one might intuit that variation  
347 within salinity especially would be greater at that location but it was not observed.  
348 Lewis et al., [2011] suggested that snow thickness was a key component in regulating  
349 the heat fluxes and morphological changes in the sea ice during our study. The ice at  
350 the Brussels site had little snow accumulation (Figure 2) and larger temperature  
351 changes than the Liège site (Figure 4) where the snow cover was thicker and  
352 insulated the underlying sea ice cover. Indeed, snow has a low thermal conductivity,



353 about an order of magnitude lower than that of sea ice, and therefore acts as a  
354 thermal insulator [Massom *et al.*, 2001].

355 The presence of a thick snow cover also provided overburden that resulted in  
356 negative freeboard (Figure 2). The negative freeboard observed at the Liège site  
357 toward the end of our study, associated with a permeable sea ice cover with an  
358 interconnected brine network, caused flooding of the ice surface and formed a saline  
359 slush layer [Lewis *et al.*, 2011]. Nutrient distribution data in the sea ice further  
360 confirmed that flooding occurred [Brabant 2012].

361 b. Physical controls on inorganic carbon in sea ice

362 Larger sea ice temperatures changes observed at the Brussels site were  
363 associated with generally higher brine salinities (Figure 4 and 5), higher TA,  $TCO_2$ ,  
364 and *in situ*  $pCO_2$  and lower  $pH_T$  (Figure 5) compared to the Liège site. These  
365 differences were expected because most solute concentrations increase with brine  
366 salinity, which also decreases  $CO_2$  solubility [Papadimitriou *et al.*, 2004]. As the  
367 temperature changes were mainly observed in the upper layer of the ice cover, the  
368 differences in salinity, TA,  $pH_T$ ,  $TCO_2$  and  $pCO_2$  between the upper and lower brine  
369 samples were greater at Brussels than at Liège (Figure 5). However, it is surmised  
370 that vertical redistribution of brine between 1 and 6 October homogenized brine  
371 salinity, TA,  $pH_T$ ,  $TCO_2$  and  $pCO_2$  between the two-sackhole depths sampled on 6  
372 October. Sea ice temperature decreased between 11 and 16 October increasing the  
373 upper brine salinity and TA (Figure 5) while the brine volume shrank below the 5%  
374 level (Figure 4), which in theory should indicate impermeability of the sea ice  
375 [Golden *et al.*, 2007] at that thickness, isolating the upper brine layer from those

376 below. Therefore, large differences were observed in salinity, TA,  $TCO_2$  and  $pH_T$   
377 between the upper layer and lower brine samples. At Liège, thermal fluctuations in  
378 the ice cover were limited by thicker snow cover, resulting in small differences in  
379 salinity, TA,  $pH_T$ ,  $TCO_2$  and *in situ*  $pCO_2$  between the upper and lower brine sample  
380 depths (Figure 5).

381 Brine  $pCO_2$  and, to a lesser extent, bulk ice  $pCO_2$  both seem to follow the  
382 observed cyclical variations in the ice temperatures (Figure 6) indicating that the  
383 dilution – concentration effect in large part controls the  $pCO_2$ . As the ice cover cooled  
384 the  $pCO_2$  increased slightly (*e.g.*, on 6, 16 October at the Brussels site and on 18  
385 October at the Liège site; Figures 4 and 5). Conversely,  $pCO_2$  dropped as  
386 temperatures rose (*e.g.*, on 11 and 21 October at Brussels and on 23 October at  
387 Liège). Because  $pCO_2$  is highly dependent on temperature, the changes in both brine  
388 and bulk ice  $pCO_2$  were larger at the Brussels site than at the Liège site (due to the  
389 increased insulation provided by the snow cover in the latter). In addition, greater  
390 changes in brine volume content throughout the ice column at the Brussels site  
391 (Figure 4) led to more variability in brine  $pCO_2$  than in the bulk ice due to the effects  
392 of brine dilution – concentration (Figure 6). At the Liège site, the  $pCO_2$  variations  
393 were limited by small variations in ice temperature under the thicker snow cover  
394 (Figure 4). Surface flooding on 18 and 23 October, might have hydrostatically forced  
395 high  $pCO_2$  seawater laterally or upward through the ice matrix. An increase of the *in*  
396 *situ* brine  $pCO_2$  and TA was observed on 18 October but these parameters decreased  
397 on 23 October (Figure 5-6). Therefore, the TA and  $pCO_2$  fluctuations observed  
398 between the 18 and 23 October could also be solely explained by the changes in the

399 thermal regime (cooling and then warming). Brine salinity seems to be the main  
400 control on the brine carbonate system; both  $nTA$  and  $nTCO_2$  from both stations were  
401 relatively constant through most of the sampling period. The small scatter in the  
402  $nTCO_2$  concentrations could simply be due to errors in calculating  $nTCO_2$  from  $TA$   
403 and  $pH_T$ . Further, the general agreement between the measured and calculated brine  
404  $pCO_2$  values (Figure 5) seems to support the assumption that the equilibrium  
405 constants are valid at subzero temperatures and high salinities [Marion 2001; Delille  
406 *et al.*, 2007]. Only on 1 October did the measured and calculated brine  $pCO_2$  values  
407 differ substantially, possibly because of errors in any of the measured parameters on  
408 that first day of sampling.

409 The *in situ* brine  $pCO_2$  values are more variable than those in bulk ice (Figure 6).  
410 Sampling brine using the sackhole technique provides the advantage of a direct *in*  
411 *situ* measurement, but the origin of the brine that collects in the sackhole is  
412 unknown, and only brine that can move easily within the ice matrix is sampled. In  
413 addition, sackholes are subject to air-sea exchange during sampling, so the low  $pCO_2$   
414 brine could well have absorbed at least some  $CO_2$  from the air above it before we  
415 completed our measurements. Brine collected using the sackhole technique  
416 represents interconnected liquid brine inclusions, in the form of relatively large  
417 brine channels susceptible to mixing with the underlying, high  $pCO_2$  seawater due to  
418 the flooding or other types of vertical redistribution. In comparison, our bulk ice  
419  $pCO_2$  analyses address brine at a well-defined location within the sea ice and include  
420 both brines and gas bubbles trapped within the ice matrix. It should be stressed that  
421 small isolated brine pockets trapped and isolated in the ice matrix are not sampled

422 using the sackhole technique but are nevertheless included in the bulk ice  $p\text{CO}_2$   
423 measurement. In addition, the sackhole technique has a poor resolution as it  
424 integrates brine through the all sackhole depth while the resolution of the bulk ice  
425  $p\text{CO}_2$  is significantly better as the measurement is performed on a ice sample size of  
426 (4 x 4 x 4.5 cm). On the other hand, the relatively small size of the bulk ice  $p\text{CO}_2$   
427 sample might result in not including a (fast responding) brine channel, the latter  
428 typically being several centimeters apart. Therefore, changes in bulk ice  $p\text{CO}_2$  values  
429 are less variable, reflecting mostly internal melting due to temperature and resultant  
430 salinity changes in the ice cover. However, we assumed that microstructure changes  
431 due to cooling-warming processes during storage do not have any significant impact  
432 to our measurements. Sackhole brines samples highlight rapid changes in the brine  
433 network such as a cooling/warming events in the ice, input of high  $p\text{CO}_2$  seawater or  
434 from brine convection and possible contamination from contact with the  
435 atmosphere during the 10-60 minute collection time window.

### 436 **c. Biological controls on carbon dynamics within sea ice**

437 *Dumont* [2009] and *Brabant* [2012] presented a complete description of the  
438 distribution and concentration of organic matter, including chlorophyll-*a* (e.g. Figure  
439 9) in sea ice at both the Brussels and Liège sites. The vertical Chl *a* distributions were  
440 more variable at Liège site than at Brussels, but at neither site showed clear  
441 variations in Chl *a* associated with the changes in  $p\text{CO}_2$ , save for during the flooding  
442 event at Liège from 18 to 23 October, which increased Chl *a* and  $p\text{CO}_2$ . However, the  
443 presence of biology may overall contribute to the low  $p\text{CO}_2$  measured on both sea

444 ice and brine samples. The persistent opposite trends of the Chl *a* and *p*CO<sub>2</sub> profiles  
445 at Liège might reflect this contribution.

446 **d. Antarctic sea ice as a spring-time sink of atmospheric CO<sub>2</sub> – comparison**  
447 **with the Arctic.**

448 The bulk ice *p*CO<sub>2</sub> values observed during the present study in the Antarctic are  
449 within the same range as those few records existing in the Arctic at Barrow, Alaska  
450 [Geilfus *et al.*, 2012b], and Resolute Bay, Canada [Geilfus *et al.*, 2014] (Figure 10a, b),  
451 where sampling also included melting, nearly isothermal first-year landfast sea ice in  
452 late spring. Higher *p*CO<sub>2</sub> values were reported from early spring sea ice at Barrow  
453 [Geilfus *et al.*, 2012b] and from SW Greenland [Crabeck *et al.*, 2014]. Although based  
454 on limited data, Antarctic sea ice may have lower *p*CO<sub>2</sub> values than Arctic sea ice at  
455 the same ice temperature (Figure 10b, c, one-way ANOVA;  $F_{1, 210}=30.73$ ,  $p<0.001$ ),  
456 although differences in the sea ice texture and dynamical forcing between the two  
457 poles are important and may have substantial effects on permeability (and therefore  
458 fluxes) and should be further investigated. It is noteworthy that the observed range  
459 of concentrations suggests that Antarctic sea ice becomes undersaturated in CO<sub>2</sub>  
460 relative to the atmosphere early in the winter–spring transition and reaches levels  
461 not observed in Arctic sea ice until much later in the spring decay process [Geilfus *et*  
462 *al.*, 2012a,b; 2014; Crabeck *et al.*, 2014].

463 The bulk ice *p*CO<sub>2</sub> data were collected at different times of the year in the Arctic  
464 and in the Antarctic (early to late spring) under different temperature and salinity  
465 conditions. Therefore we looked at the relationship between the bulk ice *p*CO<sub>2</sub> and  
466 the brine volume (Figure 10d). At low brine volumes (due to low T and/or high S)

467 the bulk ice  $p\text{CO}_2$  is high while at high brine volumes (due to high T and/or low S)  
468 the bulk ice  $p\text{CO}_2$  is low (Figure 10d). It should also be noted that both in the Arctic  
469 and in the Antarctic, spring sea ice can become undersaturated in  $\text{CO}_2$  while the  
470 underlying seawater is supersaturated with respect to the atmosphere (Figure 7)  
471 [Papakyriakou and Miller, 2011].

472 During this study, we observed a net uptake of atmospheric  $\text{CO}_2$  by the snow and  
473 sea ice at both sites. This uptake was in the same order of magnitude as previous  
474 fluxes reported over Antarctic sea ice during the austral summer by *Delille* [2006]  
475 and *Nomura et al.*, [2013] and over Arctic sea ice by *Semiletov et al.*, [2004], *Nomura*  
476 *et al.*, [2010a,b], and *Geilfus et al.*, [2012a; 2013; 2014], using similar chamber  
477 techniques. At the Brussels site, fluxes measured over snow were similar to those  
478 measured over bare ice suggesting the thin snow cover had a limited impact on  $\text{CO}_2$   
479 exchange between the atmosphere and sea ice. At the Liège site, thicker snow cover  
480 reduced the magnitude of the fluxes. The snow cover could have acted as a buffer  
481 between the ice and the atmosphere, as suggested by *Miller et al.*, [2011]. However,  
482 in contrast to *Nomura et al.*, [2010b], a snow cover thicker than 9 cm did not seem to  
483 completely prevent the  $\text{CO}_2$  exchanges between the ice and the atmosphere.

## 484 **6. Conclusions**

485 The inorganic carbon dynamic within sea ice responds swiftly to short-term  
486 meteorological events during the SIMA expedition. The succession of warm and cold  
487 events impacted the physical properties of the sea ice and its inorganic carbon  
488 dynamics. Snow thickness modulated the heat flux to the sea ice, which impacted its  
489 salinity and therefore the sea ice carbonate system. Less snow and larger

490 temperature variations created larger variations in brine salinity, TA,  $TCO_2$ , and  
491 brine and bulk ice  $pCO_2$ . In addition, the combination of unstable salinity gradients  
492 within the ice cover and episodic warming events initiated vertical brine  
493 redistribution at the low-snow site on two occasions homogenizing brine properties  
494 vertically. At the end of the survey, flooding occurred due to snow loading at the  
495 Liège site, bringing high  $pCO_2$  seawater into the brine system.

496 During the early spring, sea ice was undersaturated and largely controlled by the  
497 brine dilution, although a potential impact of biology could contribute to the overall  
498 undersaturation. We highlighted contrasted  $pCO_2$  dynamics in bulk ice  
499 measurements as compared to sackholes measurements. The bulk ice  $pCO_2$  values  
500 were much less variable, reflecting mostly internal temperature and salinity driven  
501 thermodynamic changes while  $pCO_2$  variations in sackhole brine reflected rapid  
502 transport within an interconnected brine channel network as well as potential  
503 exchange with the atmosphere and underlying surface waters.

504 At both sampling sites, the ice cover acted as a sink for atmospheric  $CO_2$ , even  
505 despite episodic flooding by supersaturated seawater. Thus, during early spring the  
506 inorganic carbonate system in the sea ice of the Bellingshausen Sea behaved as a  
507 transition layer between the ocean and the atmosphere, reacting to atmospheric  
508 forcing and from episodic interactions with the seawater.

## 509 **7. Acknowledgments**

510 The authors are grateful to the officers and crew of the RVIB *Nathaniel B. Palmer* for  
511 their logistical assistance during the SIMBA cruise. We thank Kristel De Potter for  
512 helping with measuring the bulk ice  $pCO_2$  and Keith Johnson for his help during

513 sample collection. The SIMBA project was supported by the National Science  
514 Foundation under NSF Grant ANT 0703682 – Sea Ice Mass Balance in the Antarctic  
515 to UTSA (S.F. Ackley, PI). This work was carried out within the framework of the  
516 Belgian research program Action de Recherche Concertée “Sea Ice Biogeochemistry  
517 in a CLIMate change perspective” (ARC-SIBCLIM) financed by the Belgian French  
518 Community under contract n° ARC-02/7-318287, the BELCANTO project (contracts  
519 SD/CA/03A&B) financed by the Belgian Federal Science Policy Office, and the Fonds  
520 de la Recherche Scientifique – FNRS (FRFC 2.4649.07). N.-X. Geilfus was supported  
521 by a FRIA (Fonds pour la Recherche en Industrie Agronomiques) grant and a grant  
522 from the Arctic Research Center, Aarhus University. S. Rysgaard acknowledges the  
523 Canada Excellence Research Chair Program. B. Delille is a research associate of the  
524 Fonds de la Recherche Scientifique – FNRS. This is a Mare contribution and a  
525 contribution to the Arctic Science Partnership (ASP), [www.asp-net.org](http://www.asp-net.org).

## 526 **8. Bibliography**

- 527 Brabant, F. (2012), Physical and biogeochemical controls on the DMS/P/O cycle in  
528 Antarctic sea ice, pp. 300 pp, Universite Libre de Bruxelles, Bruxelles.
- 529 Copin Montégut, C. (1988), A new formula for the effect of temperature on the partial  
530 pressure of carbon dioxide in seawater, *Marine Chemistry*, 25, 29-37.
- 531 Cox, G. F. N., and W. F. Weeks (1983), Equations for determining the gas and brine  
532 volumes in sea-ice samples, *Journal of Glaciology*, 29(102), 306 - 316.
- 533 Crabeck, O., B. Delille, D. N. Thomas, N. X. Geilfus, S. Rysgaard, and J. L. Tison (2014),  
534 CO<sub>2</sub> and CH<sub>4</sub> in sea ice from subarctic fjord, *Biogeosciences Discuss.*, 11, 4047-4083.
- 535 Delille, B. (2006), Inorganic carbon dynamics and air-ice-sea CO<sub>2</sub> fluxes in the open  
536 and coastal waters of the Southern Ocean, 296 pp, Université de Liège, Liège.
- 537 Delille, B., B. Jourdain, A. V. Borges, J. L. Tison, and D. Delille (2007), Biogas (CO<sub>2</sub>, O<sub>2</sub>,  
538 dimethylsulfide) dynamics in spring Antarctic fast ice, *Limnology and Oceanography*,  
539 52(4), 1367-1379.



- 540 Delille, B., M. Vancoppenolle, N.X. Geilfus, B. Tilbrook, D. Lannuzel, V. Schoemann, S.  
541 Becquevort, G. Carnat, D. Delille, C. Lancelot, L. Chou, G.S. Dieckmann, J.-L. Tison  
542 (2014). Southern Ocean CO<sub>2</sub> sink: the contribution of the sea ice, *Journal of*  
543 *Geophysical Research-Oceans*, 119, doi:10.1002/2014JC009941.
- 544 Dickson, A. G., and F. J. Millero (1987), A comparison of the equilibrium constants for  
545 the dissociation of carbonic acid in seawater media, *Deep Sea Research*, 1(34), 1733-  
546 1743.
- 547 Dieckmann, G. S., and H. H. Hellmer (2010), The importance of Sea Ice: An Overview,  
548 in *Sea Ice, second edition*, edited by D. N. Thomas and G. S. Dieckmann, pp. 1-22,  
549 Wiley- Blackwell, Oxford.
- 550 DOE (Ed.) (1994), *Handbook of methods for the analysis of the various parameters of*  
551 *the carbon dioxide system in sea water*, version 2, edited by Dickson, A. G. and Goyet,  
552 C., ORNL/CDIAC-74.
- 553 Dumont, I. (2009), Interactions between the microbial network and the organic  
554 matter in the Southern Ocean: impacts on the biological carbon pump, 202 pp,  
555 Université Libre de Bruxelles, Bruxelles.
- 556 Eicken, H. (1992), Salinity Profiles of Antarctic Sea Ice - Field Data and Model  
557 Results, *Journal of Geophysical Research-Oceans*, 97(C10), 15545-15557.
- 558 Frankignoulle, M. (1988), Field-Measurements of Air Sea CO<sub>2</sub> Exchange, *Limnology*  
559 *and Oceanography*, 33(3), 313-322.
- 560 Frankignoulle, M., and A. V. Borges (2001), Direct and indirect pCO<sub>2</sub> measurements  
561 in a wide range of pCO<sub>2</sub> and salinity values (the Scheldt estuary), *Aquatic*  
562 *Geochemistry*, 7(4), 267-273.
- 563 Geilfus, N. X., G. Carnat, T. Papakyriakou, J. L. Tison, B. Else, H. Thomas, E. Shadwick,  
564 and B. Delille (2012a), Dynamics of pCO<sub>2</sub> and related air-ice CO<sub>2</sub> fluxes in the  
565 Arctic coastal zone (Amundsen Gulf, Beaufort Sea), *Journal of Geophysical Research-*  
566 *Oceans*, 117, C00G10, doi:10.1029/2011JC007118.
- 567 Geilfus, N. X., B. Delille, V. Verbeke, and J. L. Tison (2012b), Towards a method for  
568 high vertical resolution measurements of the partial pressure of CO<sub>2</sub> within bulk sea  
569 ice, *Journal of Glaciology*, 58(208), 287-300.
- 570 Geilfus, N. X., G. Carnat, G. S. Dieckmann, N. Halden, G. Nehrke, T. Papakyriakou, J. L.  
571 Tison, and B. Delille (2013), First estimates of the contribution of CaCO<sub>3</sub>  
572 precipitation to the release of CO<sub>2</sub> to the atmosphere during young sea ice growth,  
573 *Journal of Geophysical Research*, 118, 224-255, doi:10.1029/2012JC007980.

- 574 Geilfus, N. X., R. J. Galley, O. Crabeck, T. Papakyriakou, J. C. Landy, J. L. Tison, and S.  
575 Rysgaard (2014), Inorganic carbon dynamics of melt pond-covered first year sea ice  
576 in the Canadian Arctic, *Biogeosciences Discuss.*
- 577 Gleitz, M., M. R. vd Loeff, D. N. Thomas, G. S. Dieckmann, and F. J. Millero (1995),  
578 Comparison of summer and winter inorganic carbon, oxygen and nutrient  
579 concentrations in Antarctic sea ice brine, *Marine Chemistry*, 51(2), 81-91.
- 580 Golden, K. M., S. F. Ackley, and V. I. Lytle (1998), The percolation phase transition in  
581 sea ice, *Science*, 282(5397), 2238-2241.
- 582 Golden, K. M., H. Eicken, A. L. Heaton, J. Miner, D. J. Pringle, and J. Zhu (2007),  
583 Thermal evolution of permeability and microstructure in sea ice, *Geophysical*  
584 *Research Letters*, 34(16), L16501, doi:10.1029/2007GL030447.
- 585 Gran, G. (1952), Determination of the equivalence point in potentiometric titration,  
586 *Analyst, Part II*(77), 661-671.
- 587 Leppäranta, M., and T. Manninen (1988), The brine and gas content of sea ice with  
588 attention to low salinities and high temperatures, *Rep.*, Finnish Institute of Marine  
589 Research, Helsinki, 15 pp.
- 590 Lewis, M. J., J. L. Tison, B. Weissling, B. Delille, S. F. Ackley, F. Brabant, and H. Xie  
591 (2011), Sea ice and snow cover characteristics during the winter-spring transition in  
592 the Bellingshausen Sea: An overview of SIMBA 2007, *Deep-Sea Research Part II-*  
593 *Topical Studies in Oceanography*, 58(9-10), 1019-1038.
- 594 Marion, G. M. (2001), Carbonate mineral solubility at low temperatures in the Na-K-  
595 Mg-Ca-H-Cl-SO<sub>4</sub>-OH-HCO<sub>3</sub>-CO<sub>3</sub>-CO<sub>2</sub>-H<sub>2</sub>O system, *Geochimica Et Cosmochimica Acta*,  
596 65(12), 1883-1896.
- 597 Massom, R. A., R. A., Eicken, H., Haas, C., Jeffries, M. O., Drinkwater, M. R., Sturm, M.,  
598 Worby, A. P., Wu, X., Lytle, V. I., Ushio, S., Morris, K., Reid, P. A., Warren, S. G., and  
599 Allison, I.(2001), Snow on Antarctic Sea ice, *Rev. Geophys.*, 39(3), 413-445.
- 600 Mehrbach, C., C. H. Culberson, J. E. Hawley, and R. M. Pytkowicz (1973),  
601 Measurements of the apparent dissociation constants of carbonic acid in seawater at  
602 atmospheric pressure, *Limnology and Oceanography*, 18, 897-907.
- 603 Miller, L. A., M. Chierici, T. Johannessen, T. T. Noji, F. Rey, and I. Skjelvan (1999),  
604 Seasonal dissolved inorganic carbon variations in the Greenland Sea and  
605 implications for atmospheric CO<sub>2</sub> exchange, *Deep-Sea Research Part II-Topical Studies*  
606 *in Oceanography*, 46(6-7), 1473-1496.
- 607 Miller, L. A., T. Papakyriakou, R. E. Collins, J. Deming, J. Ehn, R. W. Macdonald, A.  
608 Mucci, O. Owens, M. Raudsepp, and N. Sutherland (2011), Carbon Dynamics in Sea

609 Ice: A Winter Flux Time Series, *Journal of Geophysical Research-Oceans*, 116(C02028),  
610 doi:10.1029/2009JC006058.

611 Nomura, D., H. Eicken, R. Gradinger, and K. Shirasawa (2010a), Rapid physically  
612 driven inversion of the air-sea ice CO<sub>2</sub> flux in the seasonal landfast ice off Barrow,  
613 Alaska after onset surface melt, *Continental Shelf Research*, 30(19), 1998-2004.

614 Nomura, D., H. Yoshikawa-Inoue, T. Toyota, and K. Shirasawa (2010b), Effects of  
615 snow, snow-melting and re-freezing processes on air-sea ice CO<sub>2</sub> flux, *Journal of*  
616 *Glaciology*, 56(196), 262-270.

617 Nomura, D., M. A. Granskog, P. Assmy, D. Simizu, and G. Hashida (2013), Arctic and  
618 Antarctic sea ice acts as a sink for atmospheric CO<sub>2</sub> during periods of snowmelt and  
619 surface flooding, *Journal of Geophysical Research: Oceans*, 118, 6511-6524,  
620 doi:10.1002/2013JC009048.

621 Papadimitriou, S., H. Kennedy, G. Kattner, G. S. Dieckmann, and D. N. Thomas (2004),  
622 Experimental evidence for carbonate precipitation and CO<sub>2</sub> degassing during sea ice  
623 formation, *Geochimica et Cosmochimica Acta*, 68(8), 1749-1761.

624 Papadimitriou, S., D. N. Thomas, H. Kennedy, C. Haas, H. Kuosa, A. Krell, and G. S.  
625 Dieckmann (2007), Biogeochemical composition of natural sea ice brines from the  
626 Weddell Sea during early austral summer, *Limnology and Oceanography*, 52(5),  
627 1809-1823.

628 Papakyriakou, T., and L. Miller (2011), Springtime CO<sub>2</sub> exchange over seasonal sea  
629 ice in the Canadian Arctic Archipelago, *Annals of Glaciology*, 52(57), 215-224,  
630 doi:10.3189/1727564117959315334.

631 Parmentier, F.-J. W., T. R. Christensen, L. L. Sørensen, S. Rysgaard, A. D. McGuire, P. A.  
632 Miller, and D. A. Walker (2013), The impact of lower sea-ice extent on Arctic  
633 greenhouse-gas exchange, *Nature climate change*, 3, 195-202,  
634 doi:10.1038/nclimate1784.

635 Rysgaard, S., R. N. Glud, M. K. Sejr, J. Bendtsen, and P. B. Christensen (2007),  
636 Inorganic carbon transport during sea ice growth and decay: A carbon pump in polar  
637 seas, *Journal of Geophysical Research-Oceans*, 112(C3), C03016,  
638 doi:10.1029/2006JC003572.

639 Rysgaard, S., R. N. Glud, K. Lennert, M. Cooper, N. Halden, R. J. G. Leakey, F. C.  
640 Hawthorne, and D. Barber (2012), Ikaite crystals in melting sea ice – implications for  
641 pCO<sub>2</sub> and pH levels in Arctic surface waters, *The Cryosphere*, 6, 1-8.

642 Rysgaard, S., J. Bendtsen, B. Delille, G. S. Dieckmann, R. N. Glud, H. Kennedy, J.  
643 Mortensen, S. Papadimitriou, D. N. Thomas, and J. L. Tison (2011), Sea ice  
644 contribution to the air-sea CO<sub>2</sub> exchange in the Arctic and Southern Oceans, *Tellus*  
645 *Series B-Chemical and Physical Meteorology*, 63(5), 823-830.

646 Rysgaard, S., F. Wang, R. J. Galley, R. Grimm, D. Notz, M. Lemes, N. X. Geilfus, A.  
647 Chaulk, A. A. Hare, O. Crabeck, B. G. T. Else, K. Campbell, L. L. Sørensen, J. Sievers, and  
648 T. Papakyriakou (2014), Temporal dynamics of ikaite in experimental sea ice, *The*  
649 *Cryosphere*, 8(4), 1469-1478, doi: 10.5194/tc-8-1469-2014

650 Semiletov, I. P., A. Makshtas, S. I. Akasofu, and E. L. Andreas (2004), Atmospheric CO<sub>2</sub>  
651 balance: The role of Arctic sea ice, *Geophysical Research Letters*, 31(5), L05121,  
652 doi:10.1029/2003GL017996.

653 Thomas, D. N., and G. S. Dieckmann (2010), Sea Ice - An introduction to its physics,  
654 biology, chemistry and geology, in *Sea Ice*, edited by Thomas, D. N. and Dieckmann, G.  
655 S., 2<sup>nd</sup> Edn., Science, Oxford, UK, Wiley, Blackwell, p. 621, London.

656 Tison, J. L., A. Worby, B. Delille, F. Brabant, S. Papadimitriou, D. Thomas, J. de Jong, D.  
657 Lannuzel, and C. Haas (2008), Temporal evolution of decaying summer first-year sea  
658 ice in the Western Weddell Sea, Antarctica, *Deep-Sea Research Part II-Topical Studies*  
659 *in Oceanography*, 55(8-9), 975-987.

660 Vancoppenolle, M., Timmermann, R., Ackley, S. F., Fichfet, T., Goose, H., Leonard, K.  
661 C., Lieser, J., Nicolaus, M., Papakyriakou, T., and Tison, J.-L.: Assessment of radiation  
662 forcing data sets for large-scale sea ice models in the Southern Ocean, *Deep-Sea Res.*  
663 *Pt. II*, 58, 1237–1249, 2011.

664 Weeks, W. F. (Ed.): *On Sea Ice*, Fairbanks, University of Alaska Press, Alaska, 664 pp.,  
665 2010.

666 Wettlaufer J.S., Worster M. G. and Huppert H. E. (1997), Natural convection during  
667 solidification of an alloy from above with application to the evolution of sea ice,  
668 *Journal of Fluid Mechanics*, 344, 291-316

669 Zemmeling, H. J., Delille, B., Tison, J. L., Hints, E. J., Houghton, L., and Dacey, J. W. H.:  
670 CO<sub>2</sub> deposition over the multi-year ice of the western Weddell Sea, *Geophys. Res.*  
671 *Lett.*, 33, L13606, doi:10.1029/2006GL026320, 2006.

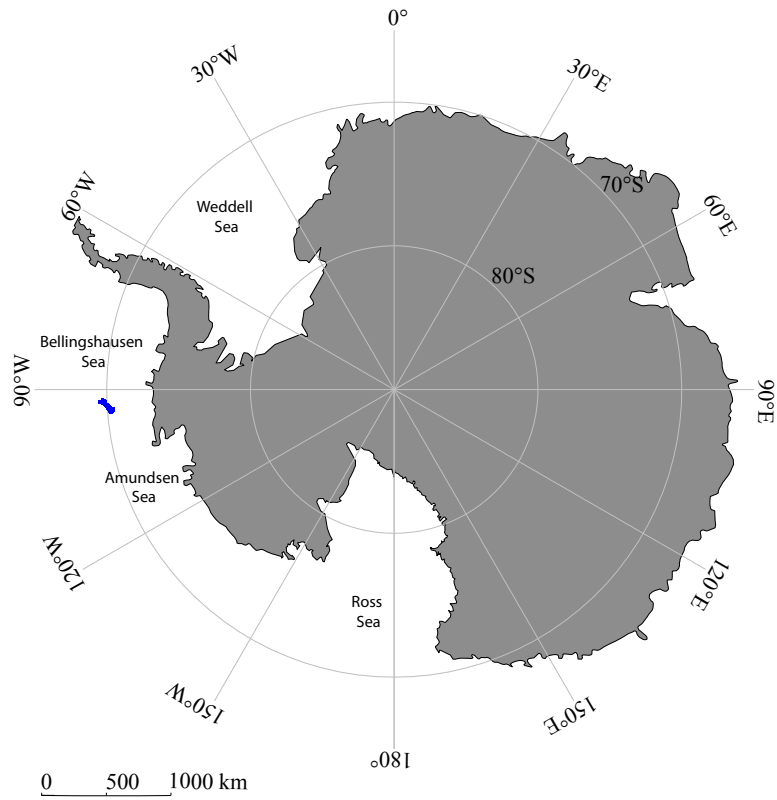
672

673

674

675 **9. Figure captions**

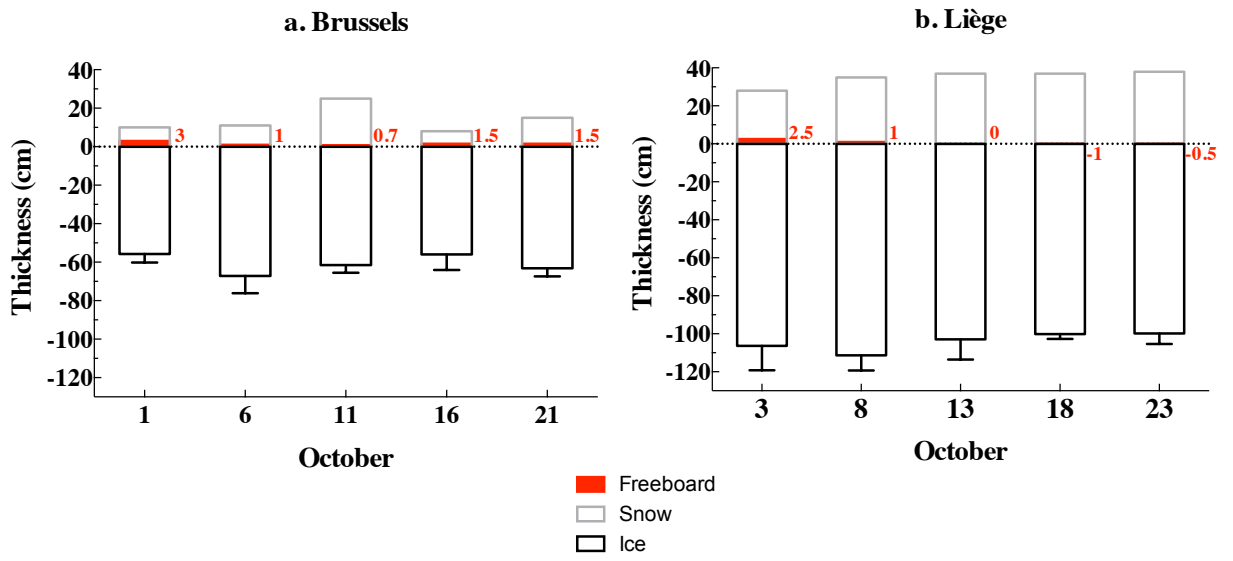
676 Figure 1: Location of the sampling area for the SIMBA cruise 2007 (blue patch), in  
677 the Bellingshausen Sea, Antarctica.



678

679

680 Figure 2: Ice (including range of observed values), snow thickness and freeboard at  
681 the Brussels and Liège sites.  
682



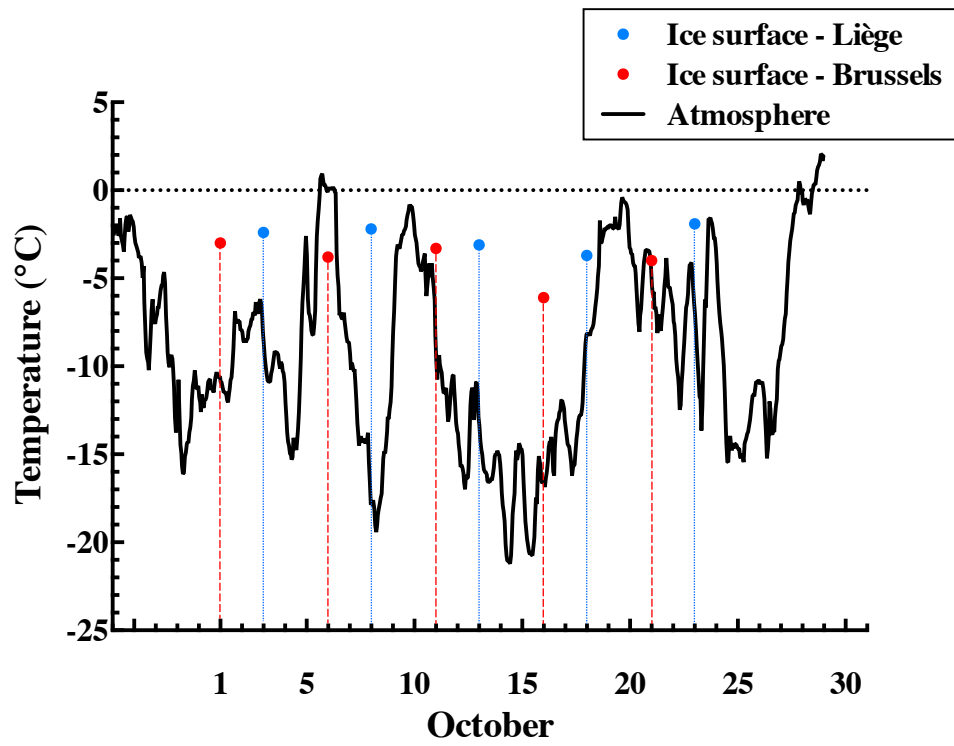
683

684

685

686 Figure 3: Daily time series of air temperature (°C) recorded on the ship and the  
687 surface ice temperature of the different sampling stations at Brussels (red  
688 dots) and Liège (blue dots) site.

689



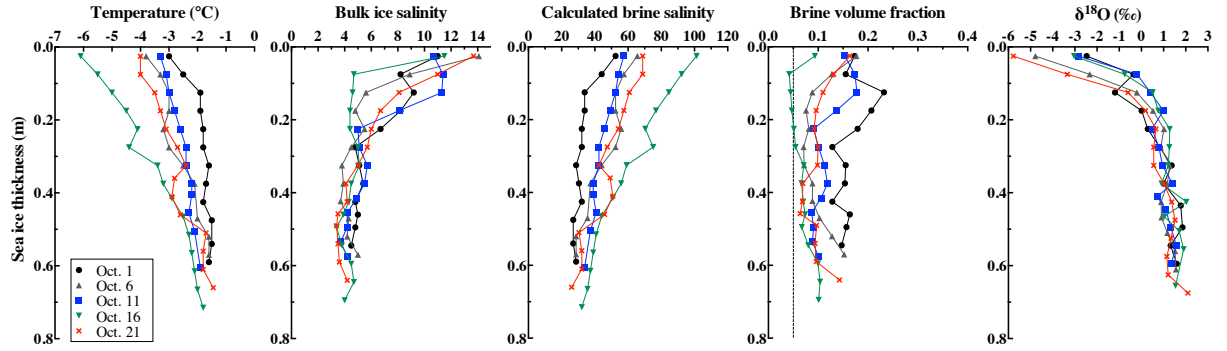
690

691

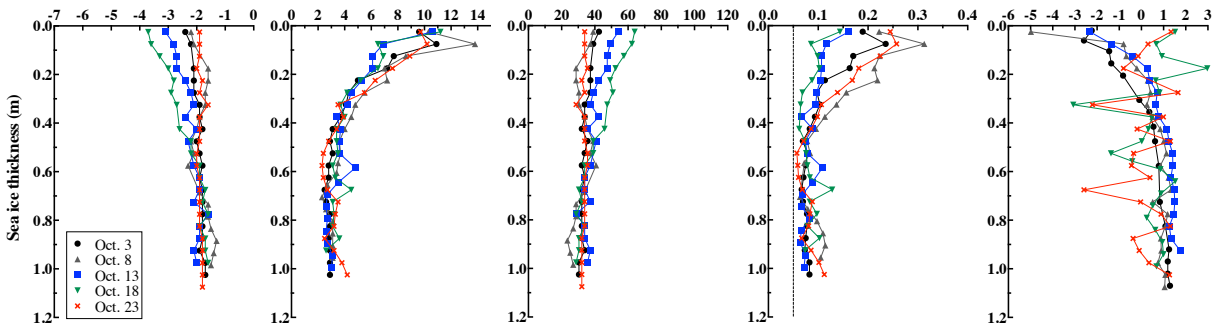
692

693 Figure 4: Profiles of temperature ( $^{\circ}\text{C}$ ), bulk ice salinity, calculated brine salinity,  
694 brine volume fraction, and  $^{18}\text{O}$  isotopic ratio from the Brussels (top) and  
695 Liège (bottom) sites.  
696

**a. Brussels**



**b. Liège**



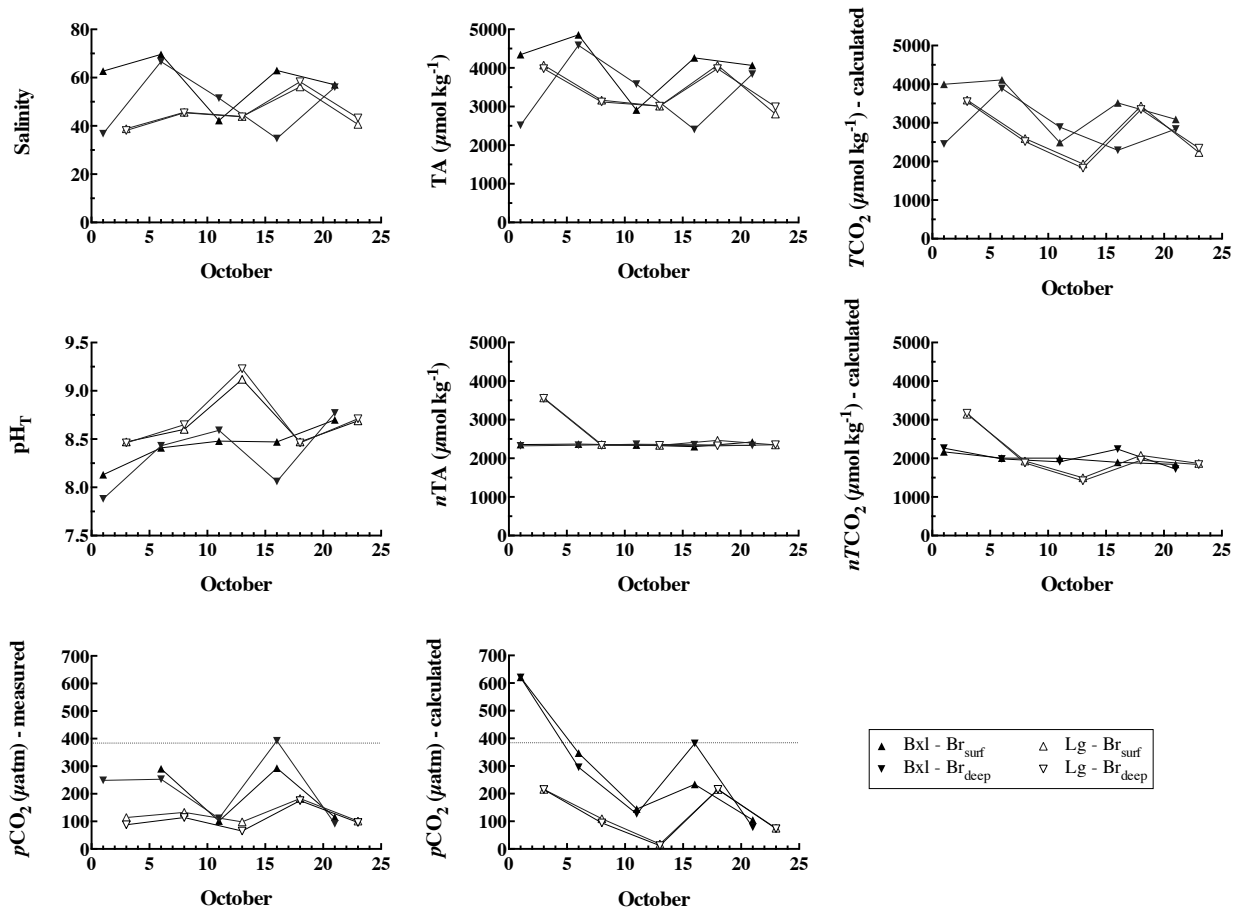
697

698

699



700 Figure 5: Evolution of salinity,  $pH_T$ , TA (in  $\mu\text{mol kg}^{-1}$ ),  $nTA$  (TA normalized to a  
 701 salinity of 34, in  $\mu\text{mol kg}^{-1}$ ), calculated  $TCO_2$  (in  $\mu\text{mol kg}^{-1}$ ) and  $nTCO_2$  ( $TCO_2$   
 702 normalized to a salinity of 34, in  $\mu\text{mol kg}^{-1}$ ), measured and calculated  $pCO_2$   
 703 (in  $\mu\text{atm}$ ) in surface and deep brine sackholes from the Brussels (Bxl) and  
 704 Liège (Lg) sites. The dotted line represents the atmospheric  $pCO_2$  in  
 705 October 2007.  
 706



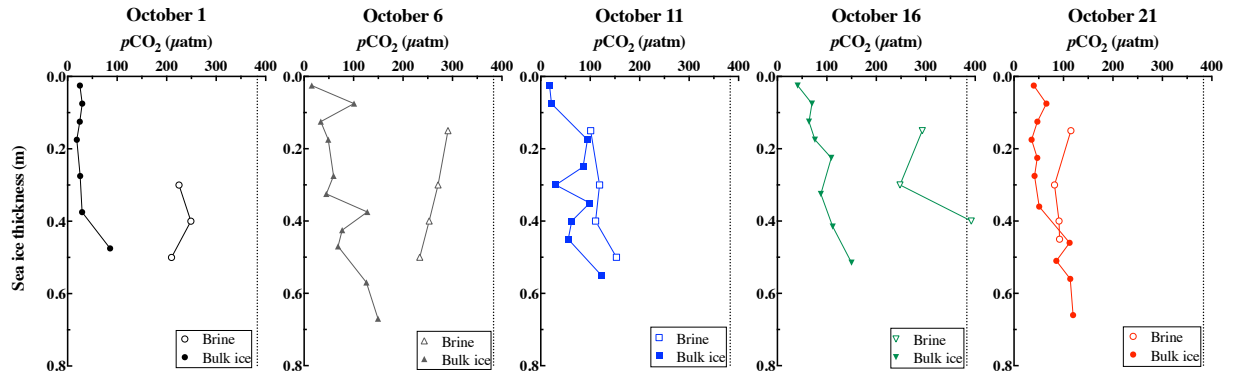
707

708

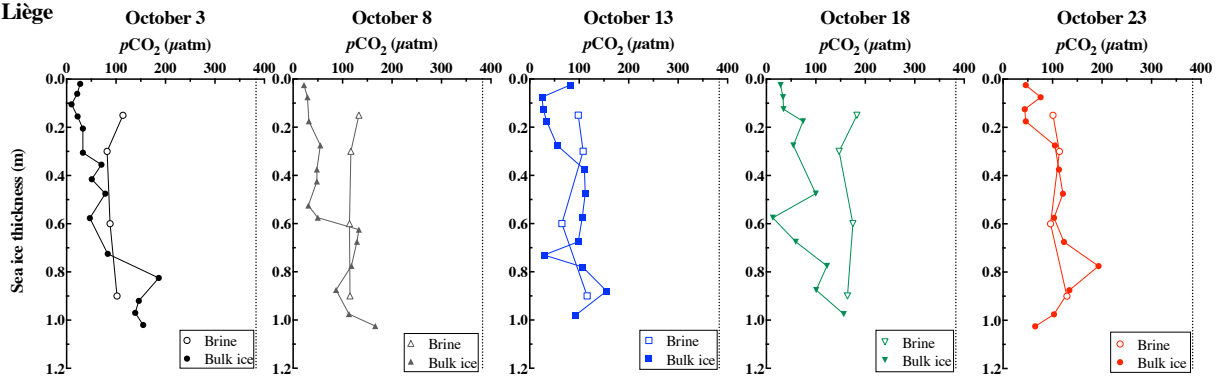
709

710 Figure 6: Vertical profiles of the *in situ* brine  $p\text{CO}_2$  (in  $\mu\text{atm}$ ) and bulk ice  $p\text{CO}_2$  (in  
 711  $\mu\text{atm}$ ) from the Brussels (top) and Liège (bottom) sites.  
 712 Data at 0.075 – 0.125 and 0.175 m depth of the station on 16 October were  
 713 measured while the brine volume was 4.1 – 4.4 and 4.6 %, respectively.  
 714

a. Brussels



b. Liège



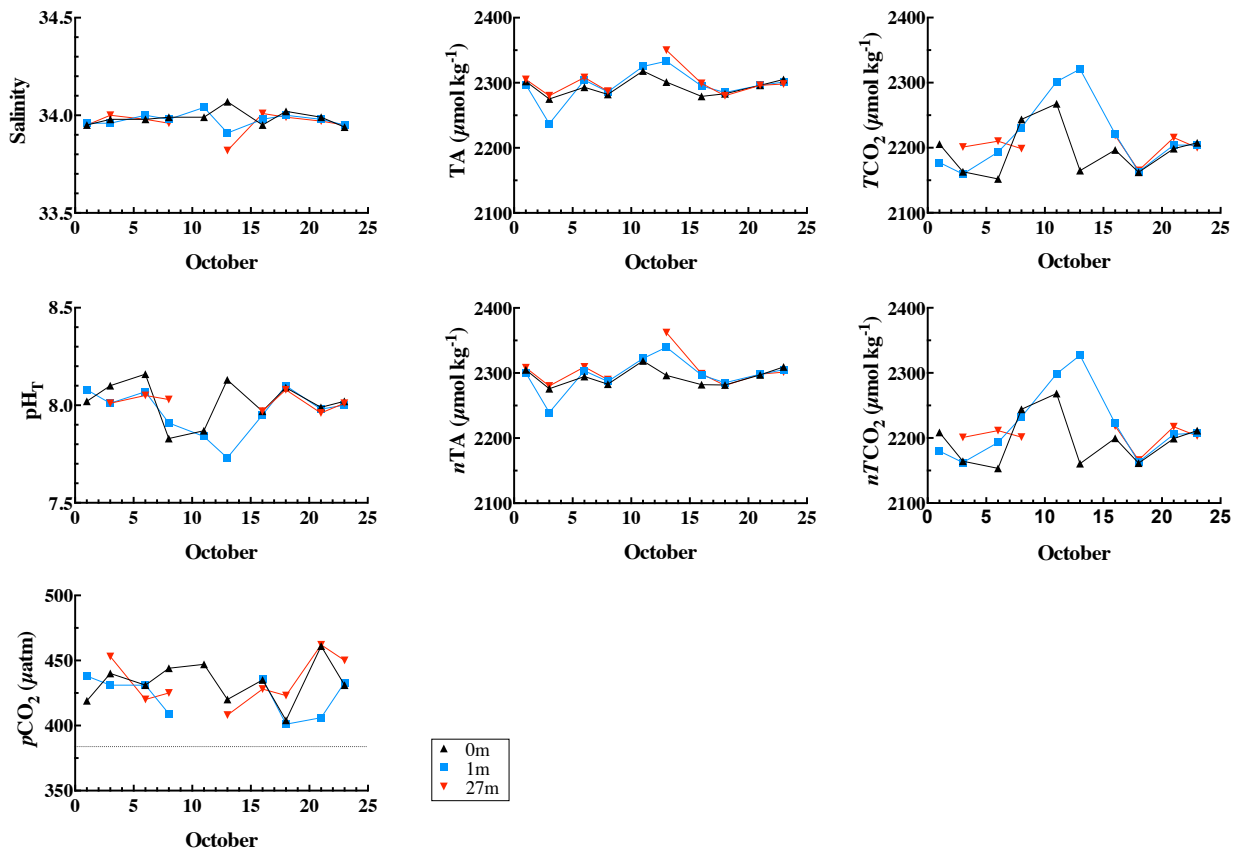
715

716

717

718 Figure 7: Evolution of salinity,  $pH_T$ , TA (in  $\mu\text{mol kg}^{-1}$ ),  $nTA$  (TA normalized to a  
 719 salinity of 34, in  $\mu\text{mol kg}^{-1}$ ), calculated  $TCO_2$  (in  $\mu\text{mol kg}^{-1}$ ) and  $nTCO_2$  ( $TCO_2$   
 720 normalized to a salinity of 34, in  $\mu\text{mol kg}^{-1}$ ), *in situ*  $pCO_2$  (in  $\mu\text{atm}$ ) in the  
 721 underlying seawater at the ice-water interface and 1 and 27m below the  
 722 ice-water interface. The dotted line represents the atmospheric  $pCO_2$  in  
 723 2007.

724

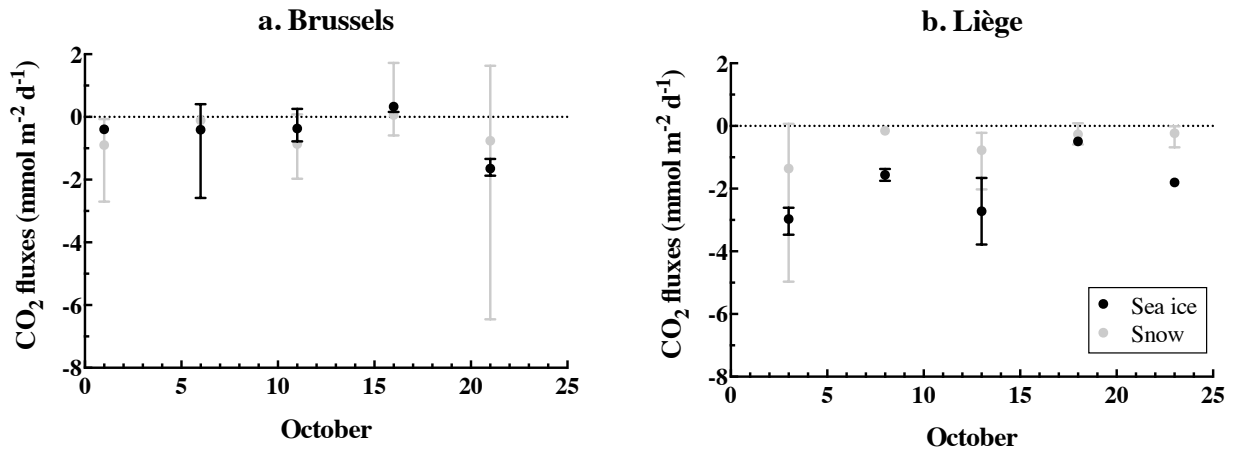


725

726

727

728 Figure 8: CO<sub>2</sub> fluxes (in mmol m<sup>-2</sup> d<sup>-1</sup>) measured over sea ice and snow for the  
729 Brussels and Liège sites.  
730



731

732

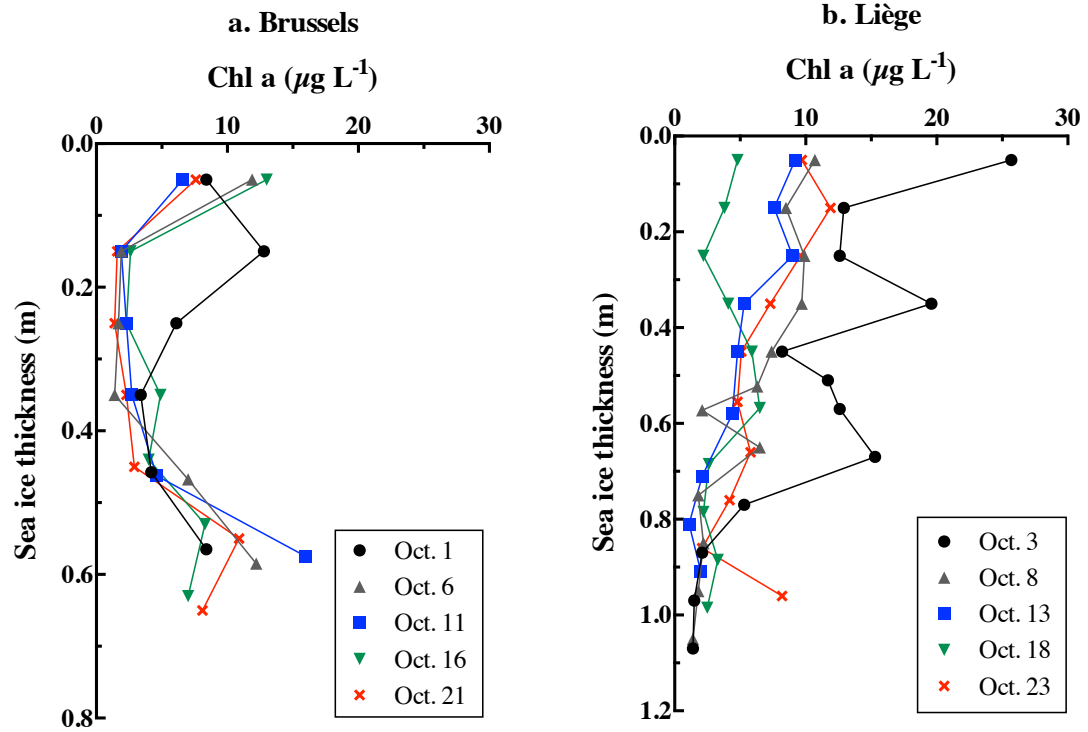
733

734

Figure 9: Profiles of Chl *a* concentration within bulk sea ice at the Brussels and Liège

735

sites, adapted from *Dumont* [2009].



736

737

738 Figure 10: a) The relationships between bulk ice  $p\text{CO}_2$  (in  $\mu\text{atm}$ ) and temperature  
739 measured in Antarctic (this study) and Arctic (Geilfus et al., 2012b; 2014;  
740 Crabeck et al., 2014) sea ice; b) Zoom in on the data from a); c) The  
741 relationships between *in situ* brine  $p\text{CO}_2$  (in  $\mu\text{atm}$ ) and brine temperature  
742 in the Antarctic (this study; Delille 2006; Delille et al., 2007) and Arctic sea  
743 ice (Geilfus et al., 2012a); d) Relationship between the bulk ice  $p\text{CO}_2$  (in  
744  $\mu\text{atm}$ ) and the brine volume fraction (in %) measured in Antarctic (this  
745 study) and Arctic (Geilfus et al., 2012b; 2014; Crabeck et al., 2014) sea ice.

